

Josephson coupling in the dissipative state of a thermally hysteretic μ -SQUID

Sourav Biswas,¹ Clemens B. Winkelmann,² Hervé Courtois,² and Anjan K. Gupta^{1,*}

¹*Department of Physics, Indian Institute of Technology Kanpur, Kanpur 208016, India*

²*Univ. Grenoble Alpes, CNRS, Grenoble INP[†], Institut Néel, 38000 Grenoble, France*

(Dated: July 17, 2018)

Micron-sized superconducting interference devices (μ -SQUIDs) based on constrictions optimized for minimizing thermal runaway are shown to exhibit voltage oscillations with applied magnetic flux despite their hysteretic behavior. We explain this remarkable feature by a significant supercurrent contribution surviving deep into the resistive state, due to efficient heat evacuation. A resistively shunted junction model, complemented by a thermal balance determining the amplitude of the critical current, describes well all experimental observations, including the flux modulation of the (dynamic) retrapping current and voltage by introducing a single dimensionless parameter. Thus hysteretic μ -SQUIDs can be operated in the voltage read-out mode with a faster response. The quantitative modeling of this regime incorporating both heating and phase dynamics paves the way for further optimization of μ -SQUIDs for nano-magnetism.

I. INTRODUCTION

A superconducting quantum interference device (SQUID), in which two Josephson junctions form a closed loop, exhibits a modulation of the critical current I_c , as a function of the magnetic flux through the loop with a period $\Phi_0 = h/2e$. It is the most sensitive magnetic field transducer to date.^{1,2} Miniaturized SQUIDs have been used for probing magnetic properties of nanoparticles³⁻⁵ and surfaces with sub- μm resolution.^{6,7} The coupling of a nano-particle's magnetic flux to a μ - or nano-SQUID is far better¹ than to a conventional SQUID, leading to a magnetic moment resolution down to below $1 \mu_B$.^{4,8} Thus, optimizing such μ -SQUIDs in terms of sensitivity, ease of fabrication and operation, or operating temperature and magnetic field range is the focus of a large panel of recent works.⁹⁻¹⁵ However, hysteresis in the current-voltage characteristics (IVCs) of μ -SQUIDs severely limits their flux resolution and speed. Hysteresis in conventional SQUIDs based on superconductor-insulator-superconductor Josephson junctions is well understood in the frame of the resistively and capacitively shunted junction (RCSJ) model.^{16,17} In contrast, hysteresis in weak-link (WL) based μ -SQUIDs arises from the Joule heating leading to a self-sustained hot-spot.¹⁸⁻²¹ Various strategies to avoid this phenomenon have been explored²²⁻²⁴ but with incomplete success. Recently, high sensitivity non-hysteretic nano-SQUIDs, based on high critical temperature cuprate grain boundary junctions shunted with gold films, have been demonstrated for nano-magnetism.^{25,26} Although such devices have some advantage as heating effects seem to be negligible there, their fabrication is quite challenging.

In a WL biased with a current I close to the critical current I_c , the transition to the dissipative state is triggered by a phase slip^{27,28}, which changes the quantum phase difference φ between the leads by 2π . The ensuing voltage peak, and thus heating, generally suffices to create an avalanche of phase-slips, driving the local WL temperature T_{WL} above the bath temperature T_b .

When the bias current is ramped down, superconductivity is recovered only at the so-called retrapping current ($< I_c$) leading to hysteresis. The hot-spot model by Skocpol, Beasley and Tinkham (SBT)¹⁸ considers that in the finite-voltage state the temperature T_{WL} is above the critical temperature T_c . The Josephson coupling is then lost so that no SQUID-type behavior is observed in this state for most of the temperature range.^{21,29,30} Still, it has been observed in some devices based on WLs^{19,31,32} and SNS junctions.³³⁻³⁵ In most cases, the theoretical modeling neglected thermal effects and relied on a conventional RCSJ model, but with an effective capacitance³⁶ well above the actual geometric one. Eventually, the SBT model was also extended to the case of a WL temperature remaining below T_c , still ignoring the WL phase dynamics.^{31,32}

Recently, some of us proposed a dynamic thermal model³⁷ of WLs, incorporating both the overheating of the WL at a temperature T_{WL} and a resistively-shunted junction (RSJ) type phase dynamics. If T_{WL} remains below T_c then the Josephson coupling across the WL is not fully destroyed. The Josephson current, together with the normal current, persists over a portion of the finite voltage branch of the IVCs,³⁸ thus leading to SQUID-type voltage oscillations. This dynamic thermal model (DTM) is in between the SBT model, where the Josephson coupling does not exist at non-zero voltages, and the R(C)SJ model that ignores the thermal effects. A similar approach was used to describe the radio-frequency response of a SNS junction.³⁹ Alternatively, hysteresis in the phase slip-controlled regime can be described using a more elaborate non-equilibrium approach using time-dependent Ginzburg-Landau equations.⁴⁰

In this paper, we report temperature- and magnetic field-dependent transport in μ -SQUIDs with a geometry optimized for a moderate Joule heating. Despite being clearly hysteretic, the devices exhibit voltage oscillations with the magnetic flux. The related non-zero flux-sensitive supercurrent contribution surviving well above the critical current, which cannot be understood using the static SBT model, is analyzed with the dynamic ther-

mal model, which quantitatively captures every observation. We eventually discuss the flux-sensitivity of the studied hysteretic μ -SQUIDs in the dynamic regime.

II. DYNAMIC THERMAL MODEL

In the dissipative state, phase slips^{28,41,42} occur at a rate $V/\Phi_0 \simeq \tau_J^{-1} = R_N I_c^0/\Phi_0$, where I_c^0 is the zero-magnetic field critical current, taken here at the bath temperature. Each phase-slip deposits a Joule heat $I\Phi_0$ leading to a temperature rise in the WL region. The Joule heat is generated over a length scale determined by the inelastic quasi-particle diffusion length,^{43,44} much longer than the WL dimensions studied here. Thus we assume a uniform²⁸ temperature over the entire WL, which determines its critical current I_c . The characteristic time for the thermal balance is $\tau_{th} = C_{WL}/k \sim$ where C_{WL} is the WL heat capacity and k is the thermal conductance to the bath. Under the quasi-static approximation, the instantaneous WL temperature \mathcal{T}_{WL} is dictated by a thermal balance between the Joule heat and the conduction to the bath $k(\mathcal{T}_{WL} - T_b)$.

If the temperature \mathcal{T}_{WL} remains below T_c at any instant of time t , the bias current I is dynamically shared between a super-current $\mathcal{I}_s(t)$ and a complementary normal current. This gives rise to a time-dependent voltage $\mathcal{V}(t) = R_N(I - \mathcal{I}_s(t))$ related to the phase difference φ through the Josephson relation $\mathcal{V}(t) = \Phi_0 \dot{\varphi}/2\pi$. The heat balance equation governing the dynamics of temperature is written as $C_{WL}\dot{\mathcal{T}}_{WL} + k(\mathcal{T}_{WL} - T_b) = \mathcal{V}^2(t)/R_N$. These two equations can be re-arranged in terms of dimensionless variables as:³⁷

$$\dot{\varphi} = 2\pi(i - i_s), \quad (1)$$

$$\alpha \dot{p} + p = \frac{\beta}{4\pi^2} \dot{\varphi}^2 \quad (2)$$

Here, the currents i and i_s are, respectively, the currents I and \mathcal{I}_s in units of the zero-magnetic field critical current $I_c^0(T_b)$. The time unit is τ_J and $\alpha = \tau_{th}/\tau_J$. The dimensionless temperature is defined as:

$$p = \frac{\mathcal{T}_{WL} - T_b}{T_c - T_b}. \quad (3)$$

We also define the dimensionless parameter

$$\beta = \frac{R_N I_c^0(T_b)}{k(T_c - T_b)} \quad (4)$$

as the ratio of Joule heat generation (at I_c^0) and heat evacuation (at T_c).

The static retrapping current⁴⁵ I_h is defined by the WL being right at the critical temperature ($\mathcal{T}_{WL} = T_c$). From Eq. 2, the thermal balance $k(\mathcal{T}_{WL} - T_b) = R_N I^2$ gives:

$$I_h = I_c^0/\sqrt{\beta}. \quad (5)$$

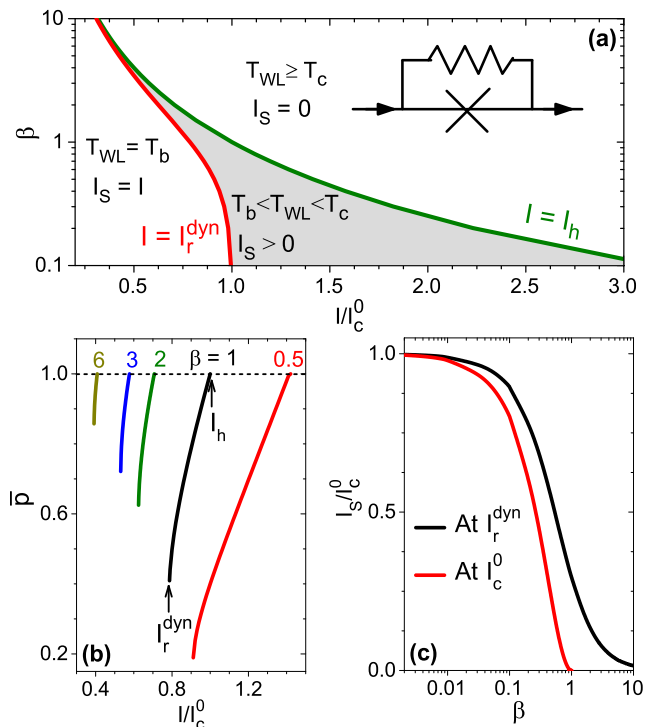


FIG. 1: Device state diagram with the grey shaded region as the dynamic regime where the WL has a finite voltage but carries a non-zero supercurrent. The region on the left of this grey-region is the zero-voltage state where all the bias current is carried as supercurrent while the right-region has no supercurrent. The red (green) line depicts the β dependence of I_r^{dyn} (I_h). Inset: Equivalent circuit of the DTM. (b) Variation of the dimensionless time-averaged WL temperature \bar{p} with the bias current in the dynamic regime for different β values. (c) Ratio of the time-averaged supercurrent I_s and the critical current I_c^0 as a function of β at the bias current values of I_r^{dyn} and I_c^0 .

At a larger current $I > I_h$ we have $\mathcal{T}_{WL} > T_c$ so that there is no Josephson coupling and hence $V = R_N I$. A non-zero supercurrent can be carried by the WL only for $I < I_h$.

The dynamic retrapping current I_r^{dyn} is the current below which the dynamic state ceases to exist and the zero-voltage state becomes stable against any phase-slip. Here and in the following, we consider WLs featuring a linear temperature dependence of the critical current and a sinusoidal current-phase relation $\mathcal{I}_s(\varphi)$. One can then obtain by solving Eqs. (1,2):³⁷

$$2\beta^2 \left[\frac{I_r^{\text{dyn}}}{I_c^0} \right]^2 = \sqrt{1 + 4\beta^2} - 1. \quad (6)$$

From numerical simulations, we find that a non-sinusoidal $\mathcal{I}_s(\varphi)$, within a regime of single-valued current, negligibly affects this relation. Moreover, the elevated WL temperature in the dynamic state gives rise to an increase in coherence length ξ and thus the current-phase relation $\mathcal{I}_s(\varphi)$ is close to sinusoidal.

The extent of the dynamic regime, defined by the current bias window $I_r^{\text{dyn}} < I < I_h$, depends on the value of the dimensionless parameter β . Figure 1(a) depicts the device state diagram found using the β dependence of I_r^{dyn} and I_h . For large values of β , i.e. poor heat evacuation and/or high I_c^0 , I_r^{dyn} and I_h are both below I_c^0 and very close to each other. The dynamic regime then occurs in a bias current window of vanishing width, making its observation in IVCs practically impossible.^{23,29} In this limit, the physics is well described by the SBT and other static thermal models.^{18,19,29} In contrast, for β of about unity or smaller, the dynamic regime spans over a significant current range. The static retrapping current I_h can then significantly exceed I_c^0 and the dynamic retrapping current I_r^{dyn} is close to I_c^0 . For extremely good heat evacuation $\beta \rightarrow 0$, one has $I_h \rightarrow \infty$, $I_r^{\text{dyn}} \rightarrow I_c^0$ and RSJ model is recovered.

In the dynamic regime between I_r^{dyn} and I_h , the WL temperature T_{WL} oscillates with time about an average value. However, for a large value of α , the magnitude of these oscillations is negligible compared to the average WL temperature.³⁷ This is always the case as τ_{th} , which can range from tens of ns to μs , is greater than τ_{J} , which is of ps order. The WL can thus be considered at a constant (time-averaged) temperature T_{WL} .^{28,37,39} The corresponding time-averaged reduced temperature \bar{p} can be calculated as a function of the current bias i from Eqs. (1, 2):³⁷

$$\bar{p} = \frac{i^2\beta^2 + \sqrt{-i^2\beta^2 + i^4\beta^2 + i^6\beta^4}}{1 + i^2\beta^2}, \quad (7)$$

with β as the single parameter. Figure 1(b) shows how \bar{p} (or equivalently T_{WL}) decreases with the current bias for various values of the parameter β , starting from 1 (or T_c) at I_h . At every bias, one can thus calculate the critical current $I_c(T_{\text{WL}})$, and the related time-averaged voltage as:

$$V = R_N \sqrt{I^2 - I_c^2(T_{\text{WL}})}, \quad (8)$$

and the time-averaged supercurrent I_s as:

$$I_s = I - V/R_N = I - \sqrt{I^2 - I_c^2(T_{\text{WL}})}. \quad (9)$$

Figure 1(c) shows I_s as a function of the parameter β at bias current values equal to I_r^{dyn} and I_c^0 . For $\beta > 1$, the time-averaged supercurrent I_s is zero when the bias current reaches I_c^0 .^{18,29} In practice, as soon as β exceeds about 2, the WL switches almost immediately to a fully normal state with $T_{\text{WL}} \geq T_c$ and (almost) zero supercurrent. For small β values, the supercurrent I_s is comparable to the full critical current I_c^0 .

III. EXPERIMENTAL DETAILS

The fabrication of the μ -SQUIDS starts with the deposition of a Nb thin film with thickness 40 nm on a Si

substrate. A resist layer was afterwards patterned using laser lithography for the outer leads and contact pads, and electron-beam lithography for the smaller structures. A 25-nm thick Al layer was then deposited followed by lift-off. The latter acting as a protective mask, the Nb devices were obtained by a SF_6 reactive-ion etch. The Al mask is eventually chemically etched. Figure 2(b) shows the loop of a SQUID with the two constrictions, of nominal width and length 40 and 160 nm respectively, in parallel. The critical current I_c was tuned down (to the 100 μA range) by trimming²⁴ down the Nb thickness to 20 (± 2) nm in subsequent reactive-ion etching steps without Al mask. The etching process can also lead to a reduction in T_c due to the appearance of a non-superconducting layer on top, bottom and also on the sides.⁴⁶⁻⁴⁸ However the thickness of such a layer^{49,50} is estimated to be ~ 2 nm only, which leaves a large and effective superconducting channel at the core of the WLs.

Electrical transport measurements were carried out in a closed-cycle refrigerator with base temperature 1.3 K. The electrical signals are thoroughly filtered, both at room temperature (π filters) and at base temperature (copper-powder filters). Home-made ground-isolated current sources and voltage amplifiers were used. From the temperature-dependent four-probe transport measurements of a first device, we find the onset of superconductivity at 8.6 K and a sheet resistance $R_{\square} = 5.8 \Omega$ in the normal state. In the following, we will present experimental data mainly from one sample. Another sample featured a similar behavior, see Appendix A.

IV. RESULTS

Zero-field current-voltage characteristics (IVCs) of a μ -SQUID at various bath temperatures T_b are shown in Fig. 2(a). The critical current I_c^0 varies strongly with temperature and exceeds 100 μA below 2 K, see Fig. 2(b). The critical current density (J_c) at 1.3 K, found as 21.1 MA/cm², is close to the Ginzburg Landau depairing current density $J_{\text{dp}} = (2/3)^{3/2}[H_c(0)/\lambda] = 36$ MA/cm² (at zero temperature), estimated using parameters for bulk and clean Nb.¹⁷ This J_c value is similar to our earlier devices.²⁹ Together with the linear dependence (up to T_h) of the critical current I_c^0 with the bath temperature T_b , this confirms the intrinsic superconducting nature of the WLs as opposed to that of SNS WLs.^{29,39,51} Below the crossover temperature $T_h \approx 3$ K, hysteresis is observed with a retrapping to the zero-resistance state at a well-defined *dynamic* re-trapping current³⁷ I_r^{dyn} , see Fig. 2(a). A fit of its temperature dependence to Eq. 6 provides the value for the critical temperature of the WL $T_c = 6.0$ K. At bias currents significantly above I_c^0 , further thermal instabilities occur in larger portions of the device as evidenced from additional re-trapping currents, see Appendix A. Our study here is focussed on the hysteretic regime and at bias currents below or in the vicinity of the critical current I_c .

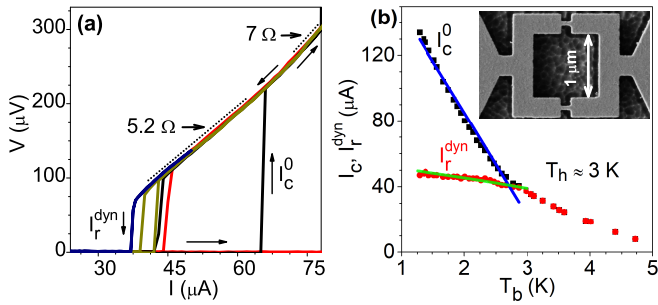


FIG. 2: (a) Current-voltage characteristics at different temperatures in the hysteretic regime. Red, black, yellow and blue colors correspond to $T_b = 1.67, 2.27, 2.77$ and 2.98 K, respectively. (b) Temperature dependence of the critical current I_c^0 and the (dynamic) retrapping current I_r^{dyn} . The crossover temperature T_h is close to 3 K. The solid lines are fits below T_h . The critical current I_c^0 is fit to $211.2(1 - T_b/3.3)$, which gives the zero-temperature critical current $I_{c0} = 211.2 \mu\text{A}$. The dynamic retrapping I_r^{dyn} is fit to Eq. 6, which gives the WL critical temperature $T_c = 6.0$ K. Inset: Scanning electron micrograph of the SQUID loop.

In the dissipative branch, the IVC slope dV/dI varies with the bias current from 5.2Ω (just above I_r^{dyn}) to 7Ω (above I_c^0) at 1.67 K, see Fig. 2(a). In the low-bias regime of interest here, the differential resistance is always close to $R_N = 5.2 \Omega$ independent of bias current and temperature, see Appendix A. This value is significantly below the value of 11.5Ω for the resistance of two WLs in parallel estimated from the sheet resistance. This indicates that the WLs are not fully resistive in this dissipative state.

When applying a perpendicular magnetic field B , and thus a flux $\Phi = B.S$, the critical current I_c displays a Φ_0 -periodic modulation, taking an effective SQUID loop area $S = 1.6 \mu\text{m}^2$. The flux modulation of the critical current, starting from its maximal zero-field value I_c^0 , is not complete and has a rather triangular shape, see Figs. 3(a,b). This behavior cannot be explained solely by asymmetric critical currents between the two arms. Moreover, self-flux related effects,¹⁶ related to the loop inductance L , are negligible here, as we estimate $LI_c^0/\Phi_0 < 0.1$. For a WL with a length $\ell \geq \xi$, the supercurrent-phase $\mathcal{I}_s(\varphi)$ relation is non-sinusoidal.^{52–55} Numerical calculations using a non-sinusoidal $\mathcal{I}_s(\varphi)$ relation indeed yield an incomplete cancellation of I_c at $\Phi = \Phi_0/2$ (Appendix B), similar to the experimental behavior.

Strikingly, the retrapping current I_r^{dyn} also shows oscillations with the magnetic flux, see Figs. 3(a,b), in contradiction with the SBT picture of a fully normal state of the device in the dissipative state. A similar feature was observed in SQUIDs based on normal metal WLs^{33–35} but not satisfactorily explained. It constitutes a first indication that superconductive coupling is not fully suppressed by the electron heating in the dissipative branch of our hysteretic devices.

Moreover, the SQUID voltage also shows an oscilla-

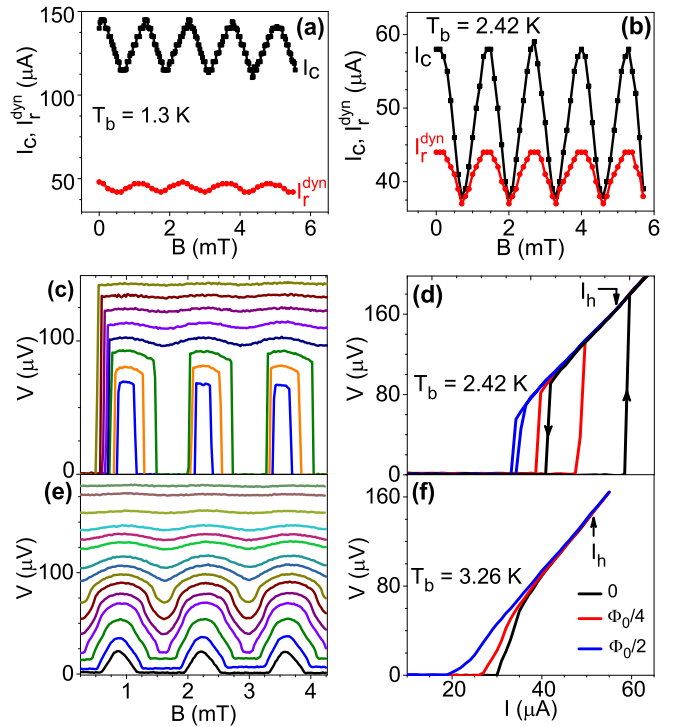


FIG. 3: (a,b) Oscillations of the critical and the dynamic retrapping currents with the magnetic field in the hysteretic regime at 1.3 and 2.42 K, respectively. (c) Voltage oscillation with magnetic field for $I = 39$ to $53 \mu\text{A}$ with $2 \mu\text{A}$ intervals at 2.42 K. (e) The same for $I = 25$ to $50 \mu\text{A}$ at 3.26 K. (d,f) IVCs at different flux values ($0, \Phi_0/2$ and $\Phi_0/4$) at 2.42 and 3.26 K, respectively.

tory dependence on magnetic field for a wide bias current window, see Figs. 3(c-f). This is completely opposed to the SBT model behavior, in which the dissipative state displays no signature of Josephson coupling across the SQUID WLs. The initial jump in voltage, seen for $I_r^{\text{dyn}} < I < I_c$ (see Fig. 3(c)), occurs due to the first arrival to the resistive branch. At a fixed temperature, the IVCs at different flux-values are found to merge on the linear branch, see Fig. 3(d,f), beyond a particular bias current. We identify this current as the *static* retrapping current I_h ,³⁷ as discussed in the model section. The $V - B$ oscillations consistently disappear at a bias current beyond I_h . At lower temperatures ($T_b = 1.3$ and 2 K) in the hysteretic regime, $V - B$ oscillations are observed over a narrow bias current span just above I_r^{dyn} , see Fig. 4 (a,b).

The flux-to-voltage transduction function V_Φ , defined as the maximum of $\partial V/\partial\Phi$, is found to be $27 \mu\text{V}/\Phi_0$ in the dynamic regime at $T_b = 2.42$ K. With a voltage noise of $\sim 1 \text{ nV}/\sqrt{\text{Hz}}$ in our circuit, this gives a flux noise density $\sqrt{S_\Phi} \approx 37 \mu\Phi_0/\sqrt{\text{Hz}}$. In the non-hysteretic regime, thanks to higher flux-to-voltage transduction V_Φ , the sensitivity $\sqrt{S_\Phi}$ reaches $3 \mu\Phi_0/\sqrt{\text{Hz}}$ at $T_b = 3.26$ K. The latter value is similar to the ones reported in non-hysteretic μ -SQUIDs with room tempera-

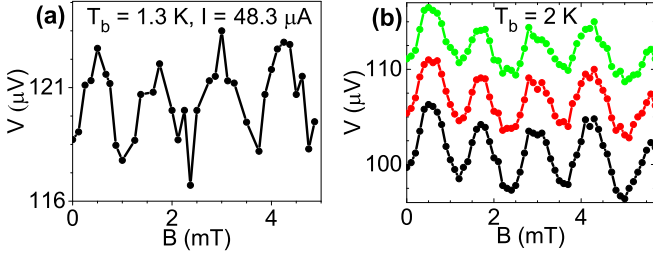


FIG. 4: (a) $V - B$ oscillation at the lowest temperature of 1.3 K at a bias current 48.3 μA just above the dynamic re-trapping current I_r^{dyn} . (b) Same at 2 K for three different bias currents (45, 46 and 47 μA) very close to I_r^{dyn} . At these lower temperatures, voltage values are extracted from IVCs at different magnetic field values.

ture amplifiers.^{1,56}

V. DISCUSSION

For modeling the μ -SQUID, we assume both WLs to be identical, with a temperature-dependent critical current $I_c^0/2$, a temperature-independent normal-state resistance $2R_N$, and a heat-loss coefficient $k/2$. The two WLs' phases φ_1 and φ_2 maintain a constant difference $\varphi_1 - \varphi_2 = 2\pi\Phi/\Phi_0$, forced by the magnetic flux through the SQUID loop. Consequently, the two WLs' average temperatures are identical in the dynamic steady state. Eventually, the SQUID behaves as a single WL with normal resistance R_N , heat loss coefficient k and critical current $I_c(T_{\text{WL}}, \Phi) = I_c^0(T_{\text{WL}}) |\cos(\pi\Phi/\Phi_0)|$. The flux-modulation of the critical current alters the expression for the dynamic re-trapping current into

$$\frac{I_r^{\text{dyn}}(\Phi)}{I_c^0} = \frac{\sqrt{\sqrt{1 + 4\beta^2 \cos^4(\pi\Phi/\Phi_0)} - 1}}{\sqrt{2}\beta |\cos(\pi\Phi/\Phi_0)|}. \quad (10)$$

At zero flux, this expression matches with Eq. 6. In the limit of a small β , one recovers the usual $|\cos(\pi\Phi/\Phi_0)|$ modulation. In contrast, I_h is independent of the flux.

For every bath temperature, we use Eq. 6 of the DTM with the measured zero-flux dynamic re-trapping current I_r^{dyn} and critical current I_c^0 to extract the value of β . Figure 5(a) shows how the parameter β varies with the bath temperature T_b over the hysteretic regime, from close to zero at T_h to about 8 at 1.3 K. For small β values, I_r^{dyn} and I_c^0 are (almost) indistinguishable in IVCs. Thus the error bars in β increases when T_b is increased towards T_h , see Fig. 5(a) and the method cannot be used beyond. As discussed below, the variation of the residual supercurrent with the bias current is then a more appropriate method to extract the value of β . The temperature coefficient of the measured critical current $I_c^0(T_b)$ below T_h being known (see Fig. 2(b)), we use Eq. 4 with k as the single free parameter to fit the $\beta(T_b)$ curve. We obtain $k = 2.6$ nW/K. Alternatively, one can also use the value

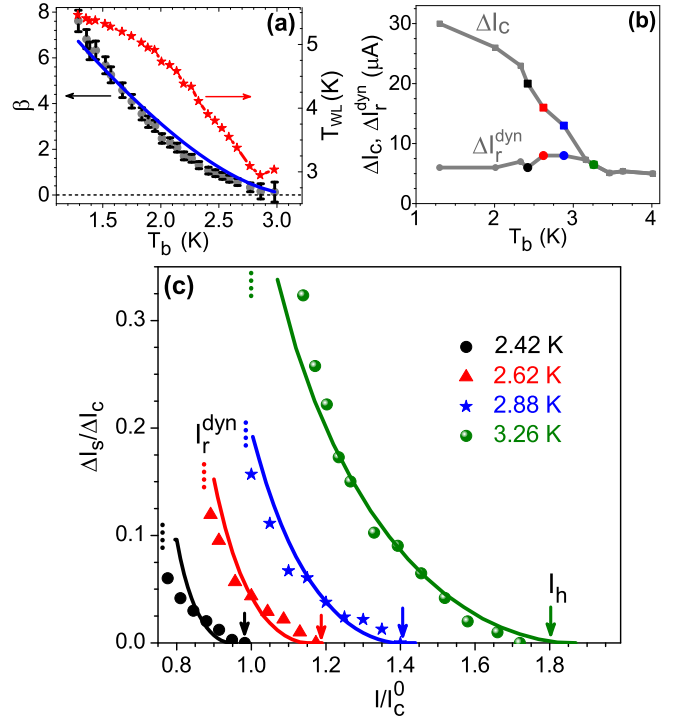


FIG. 5: (a) Black symbols: change in β with bath temperature for the measured first device as found using I_r^{dyn} and I_c^0 in the hysteretic regime (below $T_h \simeq 3$ K). The blue solid line is a fit as per Eq. 4 in DTM with $k = 2.6$ nW/K. Red symbols and line represent the WL temperature T_{WL} as a function of the bath temperature T_b and at a bias current equal to the corresponding I_r^{dyn} . (b) Variation of the modulation amplitudes ΔI_c and ΔI_r^{dyn} with bath temperature. (c) Symbols: measured supercurrent modulation amplitude $\Delta I_s/\Delta I_c$ in the dissipative state as a function of bias current ranging from I_r^{dyn} to I_h at different bath temperatures. Solid lines: best fit to the DTM with fit parameters listed in Table I. The value of I_c^0 , setting the x-axis scale, depends on the bath temperature. Arrows and dotted lines indicate the positions of the static and dynamic re-trapping current $I_r^{\text{stat/dyn}}$ respectively.

of $I_c^0 R_N/kT_c = 13.9$ obtained from the fit of the dynamic re-trapping current as a function of the bath temperature $I_r^{\text{dyn}}(T_b)$, which gives $k \approx 2.8$ nW/K. Using a typical value of heat-transfer coefficient as 5 W/cm².K,^{21,29} and these two close values of k , the effective heat loss area is estimated to be ~ 0.06 μm^2 which is larger than but still comparable to the 0.16×0.04 μm^2 area of the WL.

Using the variation of the parameter β as a function of the bath temperature T_b , Eq. 7 provides us with the behavior of the WL temperature T_{WL} at a bias current equal to the corresponding dynamic re-trapping current I_r^{dyn} , see Fig. 5(a). At the crossover temperature T_h where β is small, the WL is at thermal equilibrium with bath, i.e. $T_{\text{WL}} \approx T_b$ as in the isothermal RSJ model. Towards low temperature, the WL temperature T_{WL} increases towards T_c .

A small β value, required for observation of the dy-

dynamic regime, necessitates a small critical current I_c and/or a large thermal conductance to the bath k . Compared to earlier similar devices²⁹ for which we estimate β to be about 20 at 4.2 K, we enhanced k by widening the leads right outside the SQUID loop, while still keeping a short and narrow neck between the SQUID loop and the wide leads to avoid vortices between the two WL's current path.⁵⁷ As described earlier, we reduced I_c approximately by an order of magnitude by trimming the Nb thickness down, which overall dominates the decrease in β value. The value $\beta = 2$ obtained at 2.1 K, see Fig. 5(a), approximately defines the low temperature limit for practical operation of the SQUID in the voltage-modulation mode, significantly below the hysteresis temperature T_h . At lower temperatures, the bias-current range of dynamic regime is narrow and the voltage oscillations of small amplitude.

In the experiment, and as discussed above, the critical current is not fully modulated by the flux, which implies the same for the supercurrent. Thus one cannot compare directly the supercurrent calculated from the model to the one deduced from the measured voltage oscillations. We consider the amplitude of the supercurrent modulation in units of the critical current modulation by the flux, i.e. $\Delta I_s/\Delta I_c$. From the experimental data, we calculate $\Delta I_s/\Delta I_c$ as being equal to $\Delta V/(R_N \Delta I_c)$ where ΔV and ΔI_c are the modulation amplitude of, respectively, the voltage and the critical current. As for the theory, we calculate:

$$\frac{\Delta I_s}{\Delta I_c} = \frac{I - \sqrt{I^2 - I_c^2(T_{WL})}}{I_c^0(T_b)} \quad (11)$$

with the temperature T_{WL} being found using Eq. 7 with β as the single adjustable parameter.

Figure 5(c) shows the experimental (symbols) and theoretical (lines) values of the ratio $\Delta I_s/\Delta I_c$ as a function of the normalized bias current capturing most of the dynamic regime. A very good quantitative agreement is obtained. The fit values of β listed in Table I agree well with those deduced, and plotted in Fig. 5(a), from the analysis of the dynamic retrapping current. The comparison made here is fully justified only in the case of a sinusoidal $I_s(\varphi)$. Extending this to the case of a non-sinusoidal current-phase relation is intuitive but still not fully theoretically established. Still, the successful comparison of experimental data and theoretical calculation demonstrates that the DTM describes accurately the transition between the isothermal Josephson junction behavior and the electronically-overheated and hysteretic μ -SQUID behavior.

The insights gained from the above study, in particular the key role of the parameter β , provide a guideline for designing devices with improved performance. While for $0.4 < \beta < 2$ a wide dynamic regime is obtained, featuring both hysteretic behavior and SQUID voltage-oscillations, one needs to reach $\beta < 0.4$ so that hysteresis disappears and the voltage modulations reach a significant fraction

T_b (K)	I_c^0 (μ A)	I_r^{dyn} (μ A)	β from I_r^{dyn} value	β from Fig. 5 fit
2.42	58	44	1.13	1.1
2.62	46	40	0.66	0.74
2.88	40	38	0.35	0.5
3.26	31.6	31.6	-	0.28

TABLE I: Sample parameters including the calculated and fitted values of β for different temperatures.

of Δ/e . This is illustrated for a device in Fig. 6, with narrower WLs as compared to the previous one, resulting in a smaller critical current I_c and thus a small $\beta \sim 0.36$, even at 1.3 K.

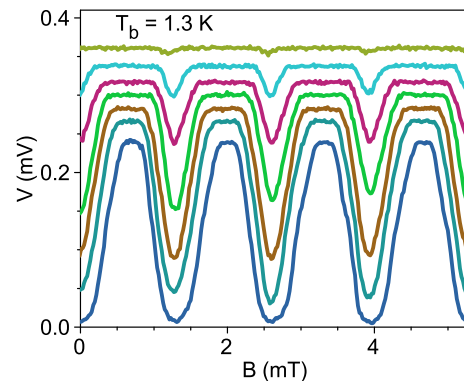


FIG. 6: $V - B$ oscillations of another device with a small critical current $I_c^0 = 51 \mu$ A and thus a small $\beta = 0.36$ at 1.3 K. Here the bias current ranges from 50 to 70 μ A.

In this device, the flux-to-voltage transduction function V_Φ is $1 \text{ mV}/\Phi_0$ at 1.3 K. With an estimated voltage noise of $1 \text{ nV}/\sqrt{\text{Hz}}$ in our circuit, we find a flux noise density $\sqrt{S_\Phi} \approx 1 \mu\Phi_0/\sqrt{\text{Hz}}$, i.e. significantly below the values of $3 \mu\Phi_0/\sqrt{\text{Hz}}$ previously reported in non-hysteretic μ -SQUIDs using room temperature amplifiers.^{1,56} The use of a low-temperature current amplifier,⁸ while voltage biasing the μ -SQUID, is expected to further improve the sensitivity.

VI. CONCLUSION

In conclusion, we discussed the crossover from the fully overheated WL, i.e. the SBT regime, where the supercurrent is either on or off, to the (isothermal) RSJ case, where the supercurrent contribution decays progressively when the bias current exceeds the critical current. This physics is relevant not only for WLs but also for Josephson junctions based on nanowires, two-dimensional materials and topological insulators, where a large supercurrent density can appear, implying a large power density at the resistive switch, together with poor heat evacuation, thus creating hysteresis. A single parameter β reflects the balance between the heat evacuation from

the WL and the injected heat, it can be tuned by trimming the critical current and/or varying the thermal coupling to the bath. This balance determines for the amplitude of voltage modulation in the phase dynamic regime. The existence of voltage oscillations makes hysteretic μ -SQUIDS useful as flux-to-voltage transducers for probing magnetism at the nanoscale with a wide bandwidth.

ACKNOWLEDGEMENTS

We are indebted to Thierry Crozes for help in the device fabrication at the Nanofab platform at Néel Institute. Help from Avijit Duley in calculating the current-phase relation is thankfully acknowledged. SB acknowledges financial support from CSIR, Government of India. AKG acknowledges a research grant from the SERB-DST of the Government of India. AKG also thanks Université Grenoble Alpes for a visiting position. CW and HC acknowledge financial support from the LabEx LANEF (ANR-10-LABX-51-01) project UHV-NEQ. We acknowledge financial support from CEFIPRA through project 5804-2.

[†] Institute of Engineering Univ. Grenoble Alpes

APPENDIX A: ADDITIONNAL EXPERIMENTAL DATA

Figure 7(a,b) shows the large scale SEM image of the μ -SQUID together with its resistance versus bath temperature ($R - T_b$) curve and non-hysteretic IVCs. The WL T_c of 6 K cannot be found from R-T plot as the bias current of 10 μ A is too high.

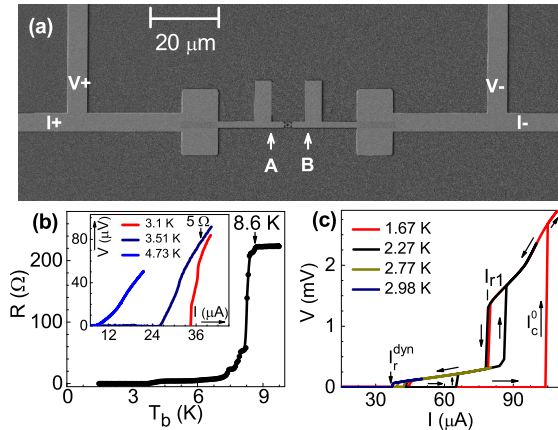


FIG. 7: (a) Larger area SEM image of the μ -SQUID showing the current and voltage leads. (b) $R - T_b$ plot at a fixed $I = 10 \mu$ A showing the superconducting transition at an onset temperature of 8.6 K. Inset shows some IVCs in the non-hysteretic regime. (c) Hysteretic IVCs over larger range of bias current showing thermal instability at I_{r1} .

Figure 7(c) shows hysteretic I-V characteristics over a large bias range. We see multiple re-trapping currents

with the larger magnitude ones representing thermal instabilities in wider portions (see arrows labeled as A and B in Fig. 7(a) of the device as evidenced from the resistance values above the respective re-trapping currents. The physics of thermal instability at higher bias currents (above I_{r1}), see Fig. 7(c), beyond the dynamic regime has been already reported by some of us.^{23,29}

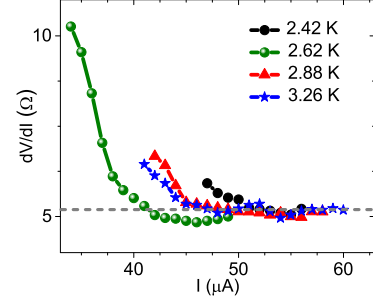


FIG. 8: The variation of the differential resistance dV/dI with I in the range $I_r^{\text{dyn}} < I$. The dotted line shows the saturation to $R_N \approx 5.2 \text{ K}$ for $I \geq I_h$.

Similar results on transport measurements observed in another (third) μ -SQUID are shown in Fig. 9(a,b). The crossover temperature T_h of this device is found to be 2.75 K. In the hysteretic regime (below 2.75 K), the retrapping current I_r^{dyn} oscillates along with I_c with B (see Fig. 9(a) for $T_b = 2.16 \text{ K}$). Estimated resistance from the linear ohmic branch of IVCs beyond I_h is 4.1 Ω . Period of oscillation is same, i.e. 1.25 mT, as that of the first device. The $V - B$ oscillations at 2.16 K are shown in Fig. 9(b) for bias currents ranging from $I = 25$ to 38 μ A.

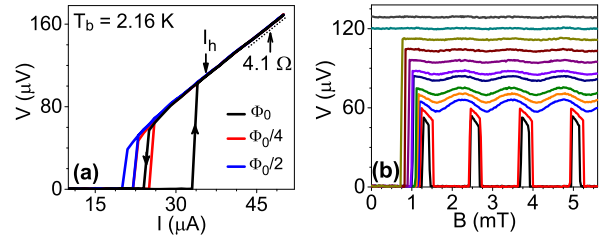


FIG. 9: (a) I_r^{dyn} oscillation with B at $T_b = 2.16 \text{ K}$ for a third μ -SQUID with $T_h = 2.75 \text{ K}$. (b) $V - B$ oscillations at this temperature for $I = 25$ to 38 μ A.

APPENDIX B: NON-SINUSOIDAL $I_s(\varphi)$ RELATION AND I_c MODULATION

As opposed to the short ($\ell \ll \xi$) WLs, where the supercurrent-phase $I_s(\varphi)$ relation is sinusoidal ($I_s = I_c \sin \varphi$),⁵⁵ the longer WLs ($\ell \geq \xi$) exhibit a non-sinusoidal $I_s(\varphi)$. Using Ginzburg-Landau theory (which is valid close to T_c), the $I_s(\varphi)$ relation for a single WL of different lengths is calculated and shown in Fig. 10.⁵² For a SQUID with identical WLs, the magnetic flux Φ gives

rise to a phase difference $2\pi\Phi/\Phi_0$ between the two WLs. Adding the two WL's supercurrents with this phase difference, we obtain the total supercurrent I_s . Figure 10(b) shows the total I_s as a function of φ at $\Phi = \Phi_0/2$. For a short WL-based SQUID, with perfectly sinusoidal $I_s(\varphi)$, this total I_s at $\Phi = \Phi_0/2$ is identically zero, which is clearly not the case for long WL based SQUIDS.

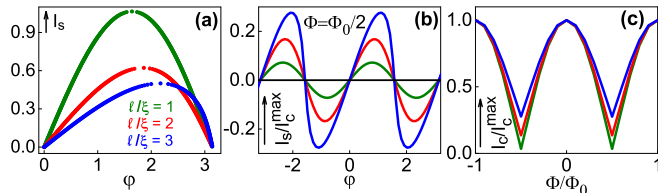


FIG. 10: (a) $I_s(\varphi)$ relation for different ℓ/ξ values. For $\ell/\xi \geq 4$, I_s is no longer single valued. (b) I_s/I_c^{\max} as a function of φ at $\Phi = \Phi_0/2$. Here I_c^{\max} is SQUID critical current at zero flux. (c) I_c/I_c^{\max} variation with flux. The green, red and blue curves, respectively, represent $\ell/\xi = 1, 2$ and 3 . The black line in (b) shows I_s for perfectly sinusoidal $I_s(\varphi)$ relation at $\Phi = \Phi_0/2$.

Figure 10(c) shows the $I_c(\Phi)$ oscillations for $\ell/\xi = 1, 2$ and 3 with I_c^{\max} as the maximum (with respect to φ) value of I_s at a given Φ . The I_c modulation amplitude decreases with increasing ℓ/ξ . This demonstrates how the I_c modulation of a SQUID with flux is limited by the non-sinusoidal $I_s(\varphi)$ relation of the WLs.

APPENDIX C: RCSJ MODEL

Here we attempt the fitting of the super-current relative modulation $\Delta I_s/\Delta I_c$ with the RCSJ model. This is anyway not very plausible due to the lack of sharp cut-off in I_s which is quite apparent in the experiments.

According to the RCSJ model,¹⁶ the current I , as shared between resistances, capacitances and the Josephson junctions of the SQUID, can be written as:

$$I = I_c^0 \sin \varphi + \frac{\mathcal{V}(t)}{R_N} + C \frac{d\mathcal{V}(t)}{dt}. \quad (12)$$

Here, $2R_N$ and $C/2$ are the resistance and capacitance of each of the two junctions. We have again assumed the screening parameter $LI_c^0/\Phi_0 \ll 1$. using the same

dimensionless quantities at Section I, we get

$$i = \sin \varphi + \dot{\varphi} + \beta_c \ddot{\varphi}. \quad (13)$$

Here $\beta_c = \frac{2\pi}{\Phi_0} I_c^0 R_N^2 C$ is the effective Stewart-McCumber parameter for the SQUID.

We get the IVCs from the numerical steady-state solutions of Eq. 13 and $V = \Phi_0 \dot{\varphi}/2\pi$. Using these solutions, we find that I_r^{dyn}/I_c^0 depends on β_c . This fact is used to extract the β_c^{calc} values for experimentally measured I_r^{dyn}/I_c^0 . Using the expression $I_s = I - V/R_N$, we have tried to fit the measured $\Delta I_s/\Delta I_c$ to the RCSJ model

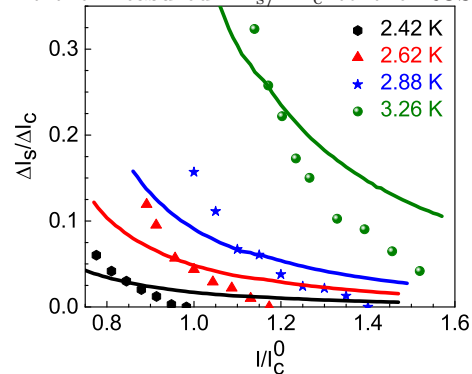


FIG. 11: Variation of residual super-current ($\Delta I_s/\Delta I_c$) in the resistive branch at $T_b = 2.42, 2.62, 2.88$ and 3.26 K as calculated from experimental data (shown by symbols). Dotted lines represent the best fit to the RCSJ model. I_c^0 in x-axis is the critical current value at zero flux for respective T_b .

in Fig. 11. The fitted β_c values are listed in Table II together with the values extracted from the values of the dynamic retrapping current I_r^{dyn} . We see from the fit that RCSJ does not fit well as compared to the DTM.

T_b (K)	I_c^0 (μA)	I_r^{dyn} (μA)	calculated β_c	fitted β_c
2.42	58	44	2.13	5.4
2.62	46	40	1.5	3.2
2.88	40	38	0.8	2.33
3.26	31.6	31.6	-	1.0

TABLE II: Comparison of measured I_r^{dyn} , I_c^0 with calculated (from I_r^{dyn} data) and fitted β_c for different temperatures.

* anjankg@iitk.ac.in

¹ C. Granata and A. Vettoliere, *Nano superconducting quantum interference device: A powerful tool for nanoscale investigations*, Phys. Rep. **614**, 1-69 (2016).

² M. J. Martínez-Pérez and D. Koelle, *NanoSQUIDS: Basics & recent advances*, Phys. Sci. Rev. **2**, 20178001 (2017).

³ W. Wernsdorfer, *Single nanoparticle measurement techniques*, J. Appl. Phys. **87**, 5094 (2000).

⁴ W. Wernsdorfer, *Classical and quantum magnetization reversal studied in nanometer-sized particles and clusters*, Adv. Chem. Phys. **118**, 99 (2001).

⁵ M. J. Martínez-Pérez, B. Müller, D. Schwebius, D. Korinski, R. Kleiner, J. Sese, D. Koelle, *NanoSQUID magnetometry of individual cobalt nanoparticles grown by focused electron beam induced deposition*, Supercond. Sci. and Technol. **30**, 024003 (2017).

- ⁶ C. Veauvy, K. Hasselbach and D. Mailly, *Scanning μ -superconducting quantum interference device force microscope*, Rev. Sci. Instrum, **73**, 3825 (2002).
- ⁷ A. Finkler, Y. Segev, Y. Myasoedov, M. L. Rappaport, L. Neeman, D. Vasyukov, E. Zeldov, M. E. Huber, J. Martin and A. Yacoby, *Self-Aligned Nanoscale SQUID on a Tip*, Nano. Lett **10**, 1046 (2010).
- ⁸ D. Vasyukov, Y. Anahory, L. Embon, D. Halbertal, J. Cuppens, L. Neeman, A. Finkler, Y. Segev, Y. Myasoedov, M. L. Rappaport, M. E. Huber and E. Zeldov, *A scanning superconducting quantum interference device with single electron spin sensitivity*, Nature Nanotech. **8**, 639 (2013).
- ⁹ L. Chen, H. Wang, X. Liu, L. Wu and Z. Wang, *A High-Performance Nb Nano-Superconducting Quantum Interference Device with a Three-Dimensional Structure*, Nano. Lett **16**, 7726 (2016).
- ¹⁰ J. E. Duvauchelle, A. Francheteau, C. Marcenat, F. Chiodi, D. Débarre, K. Hasselbach, J. R. Kirtley, and F. Lefloch, *Silicon superconducting quantum interference device*, Appl. Phys. Lett. **107**, 072601 (2015).
- ¹¹ R. Wolbing, J. Nagel, T. Schwarz, O. Kieler, T. Weimann, J. Kohlmann, A. Zorin, M. Kemmler, R. Kleiner, D. Koelle, *Nb nano superconducting quantum interference devices with high spin sensitivity for operation in magnetic fields up to 0.5 T*, Appl. Phys. Lett. **102**, 192601 (2013).
- ¹² S. Mandal, T. Bautze, O. A. Williams, C. Naud, E. Bustarret, F. Omnès, P. Rodière, T. Meunier, C. Bauerle, L. Saminadayar, *The Diamond SQUID*, ACS Nano. **5**, 7144 (2011).
- ¹³ T. Schwarz, J. Nagel, R. Wölbing, M. Kemmler, R. Kleiner, and D. Koelle, *Low-Noise Nano Superconducting Quantum Interference Device Operating in Tesla Magnetic Fields*, ACS Nano. **7**, 844 (2013).
- ¹⁴ R. Russo, E. Esposito, A. Crescitelli, E. Di Gennaro, C. Granata, A. Vettoliere, R. Cristiano and M. Lisitskiy, *NanoSQUIDs based on niobium nitride films*, Supercond. Sci. and Technol. **30**, 024009 (2017).
- ¹⁵ A. Ronzani, C. Altimiras and F. Giazotto, *Highly Sensitive Superconducting Quantum-Interference Proximity Transistor*, Phys. Rev. Appl. **2**, 024005 (2014).
- ¹⁶ J. Clarke and A. I. Braginski (Editors), *The SQUID Handbook*, 2004.
- ¹⁷ M. Tinkham, *Introduction to Superconductivity* 2nd ed. (Mc. Graw-Hill, New York, 1996).
- ¹⁸ W. J. Skocpol, M. R. Beasley and M. Tinkham, *Self-heating hotspots in superconducting thin-film microbridges*, J. Appl. Phys. **45**, 4054 (1974).
- ¹⁹ M. Tinkham, J. U. Free, C. N. Lau and N. Markovic, *Hysteretic I-V curves of superconducting nanowires*, Phys. Rev. B **68**, 134515 (2003).
- ²⁰ H. Courtois, M. Meschke, J. T. Peltonen and J. P. Pekola, *Origin of Hysteresis in a Proximity Josephson Junction*, Phys. Rev. Lett. **101**, 067002 (2008).
- ²¹ D. Hazra, L. M. A. Pascal, H. Courtois and A. K. Gupta, *Hysteresis in superconducting short weak links and μ -SQUIDs*, Phys. Rev. B **82**, 184530 (2010).
- ²² V. V. Baranov, A. G. Balanov and V. V. Kabanov, *Dynamics of resistive state in thin superconducting channels*, Phys. Rev. B **87**, 174516 (2013).
- ²³ N. Kumar, C. B. Winkelmann, S. Biswas, H. Courtois and A. K. Gupta, *Controlling hysteresis in superconducting constrictions with resistive shunt*, Supercond. Sci. and Technol. **28**, 072003 (2015).
- ²⁴ S. K. H. Lahm and D. L. Tilbrook, *Development of a niobium nanosuperconducting quantum interference device for the detection of small spin populations*, Appl. Phys. Lett. **82**, 1078 (2003).
- ²⁵ T. Schwarz, R. Wölbing, C. F. Reiche, B. Müller, M. J. Martínez-Pérez, T. Mühl, B. Büchner, R. Kleiner and D. Koelle, *Low-Noise YBa₂Cu₃O₇ Nano-SQUIDs for Performing Magnetization-Reversal Measurements on Magnetic Nanoparticles*, Phys. Rev. Appl. **3**, 044011 (2015).
- ²⁶ R. Arpaia, M. Arzeo, S. Nawaz, S. Charpentier, F. Lombardi and T. Bauch, *Ultra low noise YBa₂Cu₃O_{7- δ} nano superconducting quantum interference devices implementing nanowires*, Appl. Phys. Lett. **104**, 072603 (2014).
- ²⁷ G. Kimmel, A. Glatz, and I. S. Aranson, *Phase slips in superconducting weak links*, Phys. Rev. B **95**, 014518 (2017).
- ²⁸ N. Shah, D. Pekker and P. M. Goldbart, *Inherent Stochasticity of Superconductor-Resistor Switching Behavior in Nanowires*, Phys. Rev. Lett. **101**, 207001 (2008).
- ²⁹ N. Kumar, T. Fournier, H. Courtois, C. B. Winkelmann and A. K. Gupta, *Reversibility of superconducting Nb weak links driven by the proximity effect in a quantum interference device*, Phys. Rev. Lett. **114**, 157003 (2015).
- ³⁰ D. Hazra, J. R. Kirtley and K. Hasselbach, *Retrapping Current in Bridge-Type Nano-SQUIDs*, Phys. Rev. Appl. **4**, 024021 (2015).
- ³¹ L.-K. Wang, D.-J. Hyun, and B. S. Deaver, *Heating and flux flow in niobium variable-thickness bridges*, J. Appl. Phys. **49**, 5602 (1978).
- ³² L.-K. Wang, A. Callegari, B. S. Deaver, D. W. Barr, and R. J. Mattauch *Microwave mixing with niobium variable thickness bridges*, Appl. Phys. Lett. **31**, 306 (1977).
- ³³ V. M. Krasnov, T. Golod, T. Bauch, and P. Delsing, *Anticorrelation between temperature and fluctuations of the switching current in moderately damped Josephson junctions*, Phys. Rev. B **76**, 224517 (2007).
- ³⁴ L. Angers, F. Chiodi, G. Montambaux, M. Ferrier, S. Guéron, H. Bouchiat, and J. C. Cuevas, *Proximity dc squids in the long-junction limit*, Phys. Rev. B **77**, 165408 (2008).
- ³⁵ A. Ronzani, M. Baillegerau, C. Altimiras, and F. Giazotto, *Micro-superconducting quantum interference devices based on V/Cu/V Josephson nanojunctions*, Appl. Phys. Lett. **103**, 052603 (2013).
- ³⁶ Y. Song, *Origin of capacitance in superconducting microbridges*, J. Appl. Phys. **47**, 2651 (1976).
- ³⁷ A. K. Gupta, N. Kumar and S. Biswas, *Temperature and phase dynamics in superconducting weak links*, J. Appl. Phys. **116**, 173901 (2014).
- ³⁸ J. Bardeen, *Two-Fluid Model of Superconductivity*, Phys. Rev. Lett. **1**, 399 (1958).
- ³⁹ A. De Cecco, K. Le Calvez, B. Sacépé, C. B. Winkelmann, and H. Courtois, *Interplay between electron overheating and ac Josephson effect*, Phys. Rev. B **93**, 180505(R) (2016).
- ⁴⁰ G. Berdiyrov, K. Harrabi, F. Oktasendra, K. Gasmi, A. I. Mansour, J. P. Maneval, and F. M. Peeters, *Dynamics of current-driven phase-slip centers in superconducting strips*, Phys. Rev. B **90**, 054506 (2014).
- ⁴¹ S. L. Chu, A. T. Bollinger, and A. Bezryadin, *Phase slips in superconducting films with constrictions*, Phys. Rev. B **70**, 214506 (2004).
- ⁴² M. W. Brenner, D. Roy, N. Shah, and A. Bezryadin, *Dynamics of superconducting nanowires shunted with an external resistor*, Phys. Rev. B **85**, 224507 (2012).
- ⁴³ W. J. Skocpol, M. R. Beasley and M. Tinkham, *Phase-slip*

- centers and nonequilibrium processes in tin microbridges, *J. Low Temp. Phys.* **16**, 145 (1974).
- ⁴⁴ G. J. Dolan and L. D. Jackel, *Voltage measurements with nonequilibrium region near phase-slip centers*, *Phys. Rev. Lett.* **39**, 1628 (1977).
- ⁴⁵ Note that in the original paper introducing the DTM,³⁷ we used a different notation, I_r^{stat} , for this current.
- ⁴⁶ A. I. Gubin, K. S. Il'in, S. A. Vitusevich, M. Siegel, and N. Klein, *Dependence of magnetic penetration depth on the thickness of superconducting Nb thin films*, *Phys. Rev. B* **72**, 064503 (2005).
- ⁴⁷ I. Charaev, T. Silbernagel, B. Bachowsky, A. Kuzmin, S. Doerner, K. Il'in, A. Semenov, D. Roditchev, D. Yu. Vodolazov and M. Siegel, *Proximity effect model of ultra-narrow NbN strips*, *Phys. Rev. B* **96**, 184517 (2017).
- ⁴⁸ K. Il'in, D. Rall, M. Siegel, A. Engel, A. Schilling, A. Semenov, H.-W. Huebers, *Influence of thickness, width and temperature on critical current density of Nb thin film structures*, *Physica C* **470**, 953 (2010).
- ⁴⁹ L. N. Cooper, *Superconductivity in the Neighborhood of Metallic Contacts*, *Phys. Rev. Lett.* **6**, 689 (1961).
- ⁵⁰ Ya. V. Fominov and M. V. Feigel'man, *Superconductive properties of thin dirty superconductor-normal-metal bilayers*, *Phys. Rev. B* **63**, 094518 (2001).
- ⁵¹ P. Dubos, H. Courtois, B. Pannetier, F. K. Wilhelm, A. D. Zaikin, and G. Schön, *Josephson critical current in a long mesoscopic S-N-S junction*, *Phys. Rev. B* **63**, 064502 (2001).
- ⁵² E. de Wolf and R. de Bruyn Ouboter, *The Josephson supercurrent-phase relation*, *Physica B* **176**, 133 (1992).
- ⁵³ D. Hazra, J. R. Kirtley and K. Hasselbach, *Nano-superconducting quantum interference devices with suspended junctions*, *Appl. Phys. Lett.* **104**, 152603 (2014).
- ⁵⁴ K. Hasselbach, D. Mailly and J. R. Kirtley, *Micro-superconducting quantum interference device characteristics*, *J. Appl. Phys.* **91**, 4432 (2002).
- ⁵⁵ K. K. Likharev, *Superconducting weak links*, *Rev. Mod. Phys.* **51**, 101 (1979).
- ⁵⁶ A. G. P. Troeman, H. Derking, B. Boerger, J. Pleikies, D. Veldhuis and H. Hilgenkamp, *NanoSQUIDs Based on Niobium Constrictions*, *Nano Lett.* **7**, 2152 (2007).
- ⁵⁷ D. Pekker, A. Bezryadin, D. S. Hopkins and P. M. Goldbart, *Operation of a superconducting nanowire quantum interference device with mesoscopic leads*, *Phys. Rev. B* **72**, 104517 (2005).